https://dx.doi.org/10.21577/0103-5053.20230042

J. Braz. Chem. Soc., Vol. 34, No. 9, 1309-1316, 2023

Article

Featured Properties of the Adsorption of Tebuconazole on Ag Surface Characterized through SERS Spectroscopy

Rafael de Oliveira[a] *and Antonio Carlos Sant'Ana*[*,a]

[a]*Laboratório de Nanoestruturas Plasmônicas, Instituto de Ciências Exatas, Universidade Federal de Juiz de Fora, Rua José Lourenço Kelmer, s/n, Martelos, 36036-900 Juiz de Fora-MG, Brazil*

Pesticides present utmost importance in modern agriculture and are extensively used in countries with strong agricultural activity, such as Brazil. However, these substances are considered a significant part of environmental contamination by organic compounds. In the present work, Raman spectroscopy was employed in the vibrational characterization of the fungicide tebuconazole and surface-enhanced Raman scattering spectroscopy to the study of the adsorption of this compound on the surface of Ag nanoparticles. The proposed chemical interaction between tebuconazole and the metallic surface was inferred by relating experimental results and vibrational assignment supported by density functional theory calculations. The vibrational assignments of surface-enhanced Raman scattering spectra, by considering surface selection rules, suggest that the adsorption of the tebuconazole with Ag surface occurs by interactions of phenyl and triazole groups simultaneously. For the case of the interaction with the phenyl group, a modification of the charge distribution in the ring after adsorption was hypothesized, which was supported through the analysis of the frontier molecular orbitals of the Ag-tebuconazole complex calculated by density functional theory.

Keywords: organochloride, surface chemistry, nanostructures, triazole, plasmonic

Introduction

Pesticides are a vast class of compounds whose main function is to prevent, destroy or remedy any presence of undesirable organisms. They are intensively used mainly in agricultural production, but with other applications such as domestic use in insect control.[1] Even though there remains paramount importance of this class of compounds for world agricultural production, its misuse or excessive use, sometimes added of chemical stability, has increasingly become a major public health problem. Mostly because these substances represent a significant portion of environmental contamination by persistent organic compounds, leading to long-range transport, bioaccumulation and biomagnification in food chains.[2] Even with the awareness regarding the contamination by pesticides, their use has been growing all over the world, becoming ubiquitous environmental pollutants, and causing adverse effects to the environment (water, soil, air and living beings) and to the human health.[3,4]

Tebuconazole (TEB) is a fungicide of the triazole class, commonly included in the organochlorine class, widely applied due to its broad-spectrum antifungal activity, acting on the inhibition of the P450 enzyme and causing disruption of the fungal wall.[5,6] This fungicide has spread use in the cultivation of fruits, vegetables, nuts, and cereals, mainly for the treatment of soil and foliar infestation such as mold.[7] Due to the incorrect application of TEB, it can easily contaminate aquatic environments and soils, where it can remain for half-life times of 49 to 610 days, under aerobic conditions.[8] In addition, it can cause damage to the cultivated seeds themselves, affecting their germination,[7] possibly leading to long-term adverse effects on aquatic ecosystems. This implicates in the incidence of human cancers, as reported for human toxicity classification.[5,6]

In the last decades, surface-enhanced Raman scattering (SERS) spectroscopy, due to its outstanding capability to record unique vibrational spectral fingerprints of adsorbates, has been one of the most used techniques, with high sensitivity in the characterization, detection, and identification of several classes of compounds, in low concentration conditions. Such sensitivity is due to the so-called SERS effect, which is dependent on the phenomenon known as localized

*e-mail: antonio.sant@ufjf.br
Editor handled this article: Paula Homem-de-Mello (Associate)

surface plasmon resonance (LSPR). The LSPR transition is inherent in nanostructured materials manufactured with the coinage metals Ag, Au and Cu, which are used in the building of SERS substrates.[9,10] The LSPR extinction feature appears when both the excitation of collective oscillation modes of free electrons on the metal surface takes place and nanostructures are smaller than the wavelength of the exciting radiation.[11] Such a mechanism involved in the SERS effect is named the electromagnetic contribution, resulting from the excitation of the surface plasmon that leads to the appearance of intense electric field on the nanostructured metallic surface. One second contribution to the SERS effect is the chemical mechanism, resulting from the formation of a surface complex whose electronic transition is in resonance with the incident radiation.[2,12] SERS spectroscopy has proven to be increasingly versatile and applicable in several areas, such as the analysis of biological systems,[13-15] environmental samples or in the characterization and detection of organic pollutants.[2,16,17]

The Raman and SERS results of TEB fungicide have been obtained by Jurašeková *et al*.[18] by using hydroxylamine Ag colloid at 785 and 532 nm excitation laser lines focusing on adsorption isotherm. Their density functional theory (DFT) calculation was done for isolated TEB, which was used for Raman spectrum assignment. The followed discussion involving AgN vibration assignment was difficult since hydroxylamine was used as reducing agent in the synthesis of Ag colloid, which was coadsorbed with TEB in all experimental conditions. They cited that their experimental condition may have led to the degradation of the adsorbate.

This work presents a complete characterization of the adsorption of the fungicide TEB on Ag nanoparticle (AgNP) surfaces through Raman and SERS spectroscopies. The assignments of the vibrational modes of the compound, for Raman and SERS spectra, were performed from the results of DFT calculations of the isolated molecule and bonded to Ag_{10} cluster. Theoretical calculations were also used in a complementary way for the identification of molecular moieties responsible for the interaction in the chemisorption of TEB on the metallic surface. The main objective of the study was the characterization of the adsorption geometries of TEB adsorbed on AgNP obtained from borohydride reduction by analyses of SERS spectral patterns recorded in aqueous medium and dry films to better understand the chemical interactions of this adsorbate with the metallic surface.

Experimental

Materials and equipment

Tebuconazole ((RS)-1-*p*-chlorophenyl-4,4-dimethyl-3-(1*H*-1,2,4-triazole-1-ylmethyl)-pentan-3-ol), silver nitrate and sodium borohydride were purchased from Sigma-Aldrich (Belo Horizonte, Brazil). Glassware was cleaned by using acqua regia. All reagents were used without further purification. All solutions were freshly prepared with Milli-Q water (18.2 MΩ cm resistivity at 25 °C).

The absorption and extinction UV-Vis spectra were obtained by using an Ocean Optics USB 2000+ spectrometer (Dunedin, USA). The spectra were collected in quartz cuvettes with an optical pathlength of 0.5 cm. The Raman and SERS spectra were obtained in a Bruker dispersive Raman spectrometer, model Senterra (Ettlingen, Germany), equipped with a charge-coupled device (CCD) detector, coupled to an Olympus optical microscope model BX51 (Tokyo, Japan) and excitation laser line with wavelength at 632.8 nm from a He-Ne laser. For the acquisition of Raman and SERS spectra a 50× long distance working objective was used and the samples were subjected to 0.2 mW laser power and 5 s accumulation time.

Synthesis of AgNP

The colloidal aqueous suspension AgNP, used in the SERS analysis, was prepared according to the Creighton reduction method[19] as follow, in an ice bath under vigorous stirring, 5.0 mL of 1.0×10^{-3} mol L^{-1} silver nitrate solution was quickly added to 15.0 mL of 2.0×10^{-3} mol L^{-1} sodium borohydride solution. After the appearance of the characteristic golden yellow color due to the formation of AgNP, the stirring was turned off and the suspension was kept in the ice bath to stabilize the colloidal suspension. AgNP formation was verified by UV-Vis spectroscopy, with the sample previously diluted 1:1 in deionized water.

SERS analyses

For the SERS analyses, samples were prepared according to an adaptation of the half-and-half dilution method suggested by Darby and Le Hu:[20] 1.0 mL of 1.0×10^{-4} mol L^{-1} TEB aqueous solution was added to the 1.0 mL of AgNP suspension, and the mixture was left to rest for 2 h for better adsorption of the analyte on the metallic surface. Then, the mixture was centrifuged for 1 h at 14000 rpm, aiming to concentrate the analyte and helping the aggregation of metallic nanoparticles for the consequent formation of hot spots. After the centrifugation, 1.8 mL of the supernatant was carefully withdrawn, and the remaining volume was shaken to resuspend the AgNP. Then, 1.0 μL of the resuspended mixture was dropped onto previously cleaned aluminum foil, taken to a vacuum

chamber to dry the sample and to form a coffee ring film, which was analyzed in a Raman spectrometer. SERS analysis in aqueous suspension was also performed using the same sample preparation method, not only performing the drying step on Al surface. Such a centrifuging pre-concentration method was used since TEB has low affinity by Ag surface stabilized by borate species, do not inducing colloid aggregation, as observed by the absence of LSPR band shift when the adsorbate was added. It was not used chloride aggregation methods since it could interfere in the adsorption analysis.

Computational details

Quantum mechanical calculations were performed using the Gaussian 09 package, Revision D.01 (Wallingford, USA),[21] considering standard convergence criteria previously configured in the software. The geometry optimization of TEB was performed by DFT calculations using functional BPV86 and Pople basis set with the addition of diffuse and polarization functions, 6-311+G(2d,p) and the comparison with the geometry optimization in other levels of theory are presented in Table S1 (Supplementary Information (SI) section). In the calculations, a continuous polarizable model (IEFPCM) was used to simulate solvation, configured with dielectric constant ε = 78.355300 (water). The LANL2DZ basis set was used to optimize a cluster with ten Ag atoms (Ag_{10}) and the TEB–Ag_{10} complex, as shown in Figure 1, for the description of the inner shell and valence electrons of Ag atoms. Cartesian coordinates for the equilibrium structure of TEB and TEB–Ag_{10} complex are shown in Tables S2 and S3 (SI section).

Frequency calculations were performed at the same level of theory (at 298.15 K and 1.0 atm), characterizing the minimum or saddle point on the potential energy surface. The vibrational frequencies ($\bar{\nu}_i$) and Raman activities (A_i) were used to obtain the intensity of the normal modes of vibration (I_i) through equation 1.[22,23]

$$I_i = \frac{A_i \alpha (\bar{\nu}_0 - \bar{\nu}_i)^4}{\bar{\nu}_i \left(1 - e^{-hc\nu_i / k_B T}\right)} \quad (1)$$

where $\alpha = 10^{-12}$, $\bar{\nu}_0$ is the laser wavenumber (in cm^{-1}), h is the constant of Planck, c is the speed of light in vacuum, k_B is the constant of Boltzmann and T is the thermodynamic temperature. Full-width at half maximum of Raman band was adjusted at 5 cm^{-1}. The Raman assignment was done with the aid of Vibrational Energy Distribution Analysis 4 (VEDA 4) software.[24]

Results and Discussion

Figure 2 shows the UV-Vis spectra of the aqueous solution of TEB, the aqueous suspension of AgNP, and the mixture of TEB and AgNP after the adsorption time. In the TEB spectrum, characteristic bands are observed at 222 nm, ascribed to the triazole moiety, and around 265 nm ascribed to the phenyl ring.[25] In the AgNP extinction spectrum, an LSPR band with maximum around 400 nm is observed, indicating a narrow size distribution. The extinction spectrum of the TEB–Ag mixture shows a large decrease in the intensity of the LSPR band of metallic nanoparticles, in addition to the appearance of a broad and low-intensity band in the range of 450 to 600 nm, not observed in the spectra of isolated components of the mixture. Such a new band is indicative of a controlled AgNP aggregation, after the addition of TEB to the system and centrifugation process, since this process did not lead to an irreversible aggregation, preserving its stability during the experiment. The aggregation that

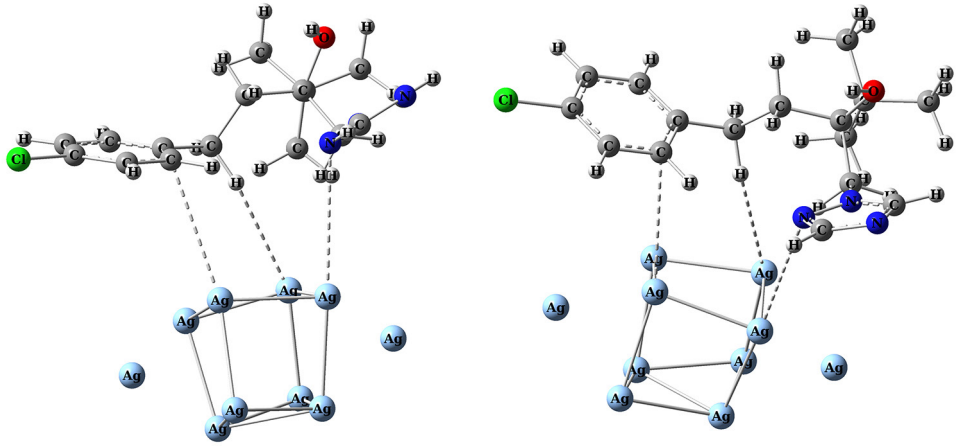

Figure 1. Two views of the optimized structure of TEB–Ag_{10} complex, with dashed lines highlighting Ag atoms nearest to the molecule.

occurred in the system is of great importance concerning the SERS analysis, being an indicative of the adsorption of TEB, since it removes part of adsorbed anions from the metallic surface, together the centrifugation that removes the excess of such not adsorbed species, which enables the formation of hot spots, most responsible for the SERS signal of the adsorbed analyte.[20]

Figure 3 shows the experimental and theoretical Raman and SERS spectra of TEB. Table 1 presents the assignment for the Raman and SERS spectra of TEB and the complete assignments of the Raman and SERS spectra are presented in Table S4 (SI section). Both SERS spectra were recorded from centrifuging pre-concentration method (Figure 2c), before and after drying process. The Raman spectrum presents more intense bands at 1597, 1210, 1091, 1012, 829, 690, 664, 641 and 589 cm^{-1}, ascribed to phenyl moiety, at 1437, 1364, 1131 and 853 cm^{-1}, ascribed to triazole moiety and at 1450, 1320, 1273 and 1230 cm^{-1}, ascribed to aliphatic moiety.

The SERS spectrum of TEB, recorded from aqueous suspension, shows more intense bands at 1440, 1360, 1293 and 972 cm^{-1}, assigned to the CN stretching of the triazole moiety, indicating such a group may perform chemical interaction with Ag surface.[26,27] In addition, the enhanced bands at 1568, 1088, 1017, 807 and 691 cm^{-1}, ascribed to phenyl moiety, are relatively less intense, suggesting such a group interacts with relative lesser strength with Ag surface than triazole one. Such inference is in agreement with the optimized geometry in DFT calculation (see Figure 1), which presents lower distance between triazole and Ag atom than phenyl ring and the other indicated Ag atom, suggesting the calculated adsorption geometry is a good model for the SERS analysis in aqueous suspension. The SERS bands at 972 and 1440 cm^{-1}, assigned to CN stretching mode, have additional contribution of CO stretching and CH_2 deformation, respectively. Another enhanced band can be observed at 1276 cm^{-1} and assigned to CH_2 wagging mode. According to DFT calculation of vibrational frequencies, these normal modes are perpendicular to the Ag surface, which can justify the observed featured enhancement of the corresponding SERS bands, in agreement with surface selection rules.[28,29] By the same rules, the presence of the band at 691 cm^{-1}, assigned to the out-of-plane deformation of the phenyl

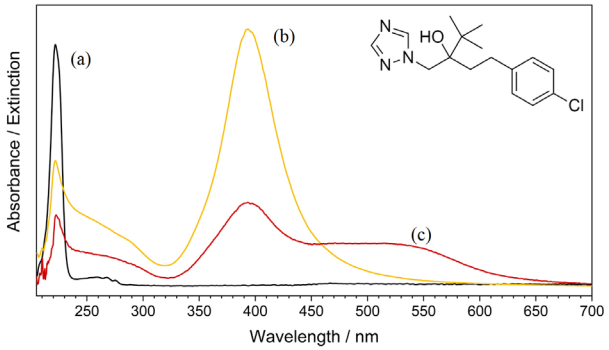

Figure 2. (a) UV-Vis absorption spectrum of the 1.0×10^{-4} mol L^{-1} TEB aqueous solution, and UV-Vis extinction spectra of AgNP aqueous suspension (b) before and (c) after the addition of TEB (final concentration: 5.0×10^{-5} mol L^{-1}). Inset: chemical structure of TEB.

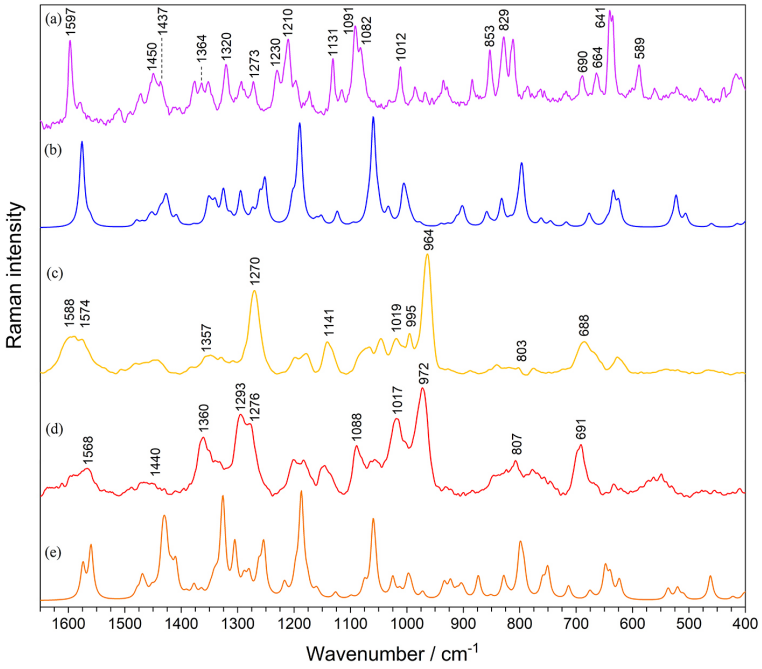

Figure 3. Raman spectra of TEB: (a) in solid state and (b) simulated spectrum; SERS spectra of TEB: (c) in dry film, (d) in aqueous suspension and (e) simulated SERS spectrum. Theoretical simulated spectra were corrected for an excitation wavelength of 632.8 nm.

Table 1. Tentative assignment of Raman and SERS bands present in the spectra of TEB, and corresponding calculated wavenumbers

Raman exp. (s) / cm^{-1}	Raman theor. (aq) / cm^{-1}	SERS exp. (dry) / cm^{-1}	SERS exp. (aq) / cm^{-1}	SERS theor. (aq) / cm^{-1}	Assignment
1597	1576	1588	1594	1574	$\nu(CC)_{PH}$
1578	1561	1574	1568	1560	$\nu(CC)_{PH}$
1450	1427	1467	–	1427	$\delta(CH_3) + \delta(CH_2)$
1437	1409	1440	1440	1410	$\nu(CN)_{TR} + \delta(CH_2)$
1364	1340	1357	1360	1338	$\nu(CN)_{TR}$
1320	1295	1330	–	1290	$\nu(CN)_{TR}$
1294	1261	1285 (sh)	1293	1263	$\nu(CN)_{TR}$
1273	1252	1270	1276	1254	$\omega(CH_2)$
1230	1203	1198	1200	1197	$\nu(CC) + \delta(CH)$
1210	1189	1184	1178	1187	$\nu(CC)_{PH}$
1131	1124	1142	1147	1127	$\nu(CN)_{TR}$
1091	1060	1082 (sh)	1088	1060	$\nu(CC)_{PH} + \nu(CCl)$
1082	1051	1067	–	1056	$\delta(CCO) + \delta(OH)$
1012	1005	1019/995	1017	997	$\nu(CC)_{PH\text{-}br}$
968	977	964	972	972	$\nu(CN)_{TR} + \nu(CO)$
853	859	840	–	851	$\nu(CO) + \gamma(CN)_{TR}$
829	832	820	823	829	$\gamma(CC)_{PH} + \gamma(CN)_{TR}$
812	796	803	807	798	$\gamma(CC)_{PH} + \nu(CC)_{tB}$
690	718	688	691	714	$\gamma(CC)_{PH}$
664	671	671 (sh)	671	670	$\gamma(CN)_{TR}$
641	634	657 (sh)	662	648	$\delta(CC)_{PH} + \gamma(CN)_{TR}$
636	625	627	628	624	$\delta(CC)_{PH}$
589	531	550	548	537	$\gamma(CC)_{PH} + \gamma(CN)_{TR}$
–	–	234	234	193	$\nu(AgAgC) + \nu(AgAgN)$
–	–	160 (sh)	160 (sh)	148	$\nu(AgC)$

SERS: surface-enhanced Raman scattering; PH: phenyl ring; TR: triazole ring; tB: *t*-butyl group; *ν*: stretching; δ: bending; γ: bending out-of-plane; ω: wagging; PH-br: phenyl ring breathing; sh: shoulder; s: solid; exp: experimental, theor: theoretical; aq: aqueous.

group, suggests that the phenyl ring plane has a preferential parallel orientation with the Ag surface.

The SERS spectrum of TEB, recorded from the dry film shows enhanced bands at 1588, 1574, 1019, 995, 803 and 688 cm^{-1}, ascribed to phenyl moiety. However, both features at 1019 and 995 cm^{-1} are assigned to phenyl breathing mode, indicating the procedure involving centrifugation and drying processes may lead to two different molecular adsorption geometries. It is noteworthy that in the Raman spectrum, the band assigned to phenyl breathing mode is observed at 1012 cm^{-1} that is a characteristic value for substituted phenyl moieties and it is in agreement with the SERS band observed at 1019 cm^{-1}. However, the presence of the feature at 995 cm^{-1} indicates there is other strong interaction of part of adsorbed molecules with the Ag surface that may change the charge distribution in the phenyl ring, involving π-interaction with Ag atoms.[30,31] The decreasing of the relative intensities of SERS bands at 803 and 688 cm^{-1}, when compared with the SERS spectrum in aqueous medium, both assigned to out-of-plane ring modes, suggests the plane of phenyl ring is more tilted in relation to the Ag surface, in agreement with surface selection rules.[28,29] In comparison with the SERS spectrum in aqueous medium, the decrease of the intensities of the bands at 1357 and 1285 cm^{-1}, as well as the shift of the band at 964 cm^{-1}, indicate triazole moiety may have more weak interaction with Ag surface in the dry film. It is not rare to observe more than one SERS spectral pattern in the literature for several chemical species,[32] which is also evident here, in the SERS analysis of TEB.[18,33] Even though, in this case, the TEB interaction with Ag surface is governed by aqueous medium, the aggregation obtained by drying process may have allowed two different adsorption geometries.

Figure 4 presents the frontier molecular orbitals resulting from the DFT optimization of the structure of the TEB–Ag_{10} complex. The highest-energy occupied molecular orbital

(HOMO) and the lowest-energy unoccupied molecular orbital (LUMO) show that the charge density is mostly on the Ag cluster. However, LUMO presents charge transfers from Ag atoms to triazole and phenyl rings, and a CH_2 group. This result is in agreement with SERS results, which present enhanced features assigned to triazole and CH_2 moieties as well as significant changes in the bands assigned to phenyl ring.

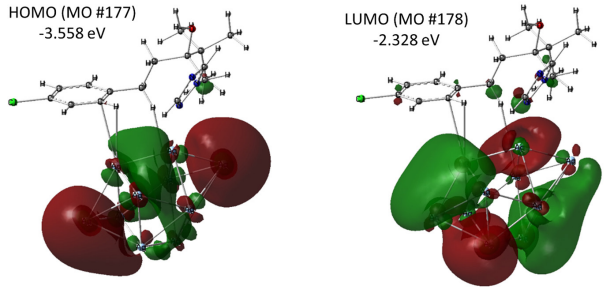

Figure 4. Frontier molecular orbitals for the DFT-optimized TEB–Ag_{10} complex.

An intense band at 1210 cm^{-1} is observed in the Raman spectrum of TEB, assigned to CC stretching of the aliphatic chain, which greatly loses its intensity in the SERS spectra. The same was verified for the band at 1082 cm^{-1}, assigned to CCO and OH in-plane deformations. In the SERS spectra, few bands are attributed to the *tert*-butyl group present in the TEB structure, probably because this group, after adsorption, is more distant from the metallic surface and its vibrational modes present components parallel to the silver surface, better visualized in the structure of the complex shown in Figures 1 and 4.

Figure 5a presents the SERS spectrum of TEB on dry film and Figure 5b shows high intensity bands, from both SERS spectra, observed in the low frequency region at ca. 234 and 160 cm^{-1}. Figure 5b presents the low wavenumber regions of both SERS spectra, in dry film and aqueous suspension. The high intensity band at 234 cm^{-1} can be assigned to the contribution of both AgC and AgN stretchings with the help of theoretical DFT calculations. However, in the literature[34,35] it is still reported a possible assignment of this band to the AgAg stretching. So, the observed band may be a superposition of different vibrational modes. Still observing Figure 5b, a low intensity shoulder is verified in SERS spectrum of the dry film around 160 cm^{-1}, which can be attributed as referring to the AgC stretching. Jurašeková *et al.*[18] assigned this feature to AgN vibration formed by the adsorption of TEB on Ag surface. However, the use of hydroxylamine as silver reducing agent precludes this ultimate assumption.

Conclusions

In the present work, SERS spectroscopy was used to characterize the adsorption of the fungicide TEB on Ag surfaces and vibrational assignment was supported by DFT calculations. The enhancement of the SERS bands ascribed to in-plane modes of triazole ring and out-of-plane modes of phenyl ring allows inferring the possible adsorption of TEB on the metallic surface through both molecular moieties, with phenyl ring done lateral π-interaction with Ag atoms. This hypothesis was reinforced by both the shifts in the ring breathing bands, observed in the SERS spectra, in comparison with the Raman spectral pattern of TEB in solid state and a possible charge transfer between Ag atoms and phenyl ring, inferred from calculated frontier molecular orbitals. Such a hypothesis for the adsorption geometry of TEB on Ag surface was reinforced by the presence of a strong SERS band around 234 cm^{-1}, which can have components from AgN and AgC stretching modes.

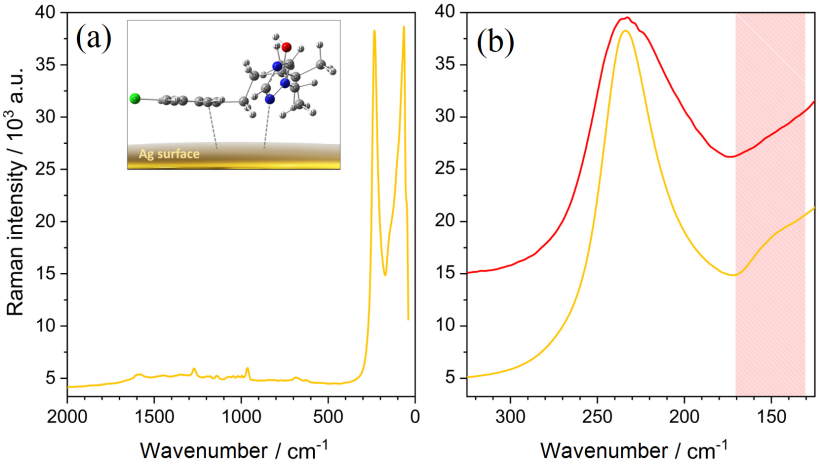

Figure 5. (a) SERS spectrum of TEB in dry film, and (b) SERS spectra in both aqueous and dry conditions, highlighted in the range of low wavenumber. Inset: proposed model for the adsorption of TEB on Ag surface.

Supplementary Information

Supplementary data (tables with calculated geometry parameters and complete assignment) are available free of charge at http://jbcs.sbq.org.br as PDF file.

Acknowledgments

The authors would like to thank CNPq and FAPEMIG (PRONEM APQ-01283-14), Brazilian Funding Agencies, by financial support. Such a study was financed in part by Coordenação de Aperfeiçoamento de Pessoal de Nível Superior - Brasil (CAPES) - Finance Code 001. The authors also thanks CNPq and CAPES for scholar fellowships.

References

1. Jayaraj, R.; Megha, P.; Sreedev, P.; *Interdiscip. Toxicol.* **2016**, *9*, 90. [Crossref]
2. Moldovan, R.; Iacob, B. C.; Farcău, C.; Bodoki, E.; Oprean, R.; *Nanomaterials* **2021**, *11*, 304. [Crossref]
3. Shattuck, A.; *J. Peasant Stud.* **2021**, *48*, 231. [Crossref]
4. Tang, F. H. M.; Lenzen, M.; McBratney, A.; Maggi, F.; *Nat. Geosci.* **2021**, *14*, 206. [Crossref]
5. Yu, L.; Chen, M.; Liu, Y.; Gui, W.; Zhu, G.; *Aquat. Toxicol.* **2013**, *138-139*, 35. [Crossref]
6. Sancho, E.; Villarroel, M. J.; Andreu, E.; Ferrando, M. D.; *Chemosphere* **2009**, *74*, 1171. [Crossref]
7. El-Naggar, M. E.; Hasanin, M.; Youssef, A. M.; Aldalbahi, A.; El-Newehy, M. H.; Abdelhameed, R. M.; *Int. J. Biol. Macromol.* **2020**, *165*, 1010. [Crossref]
8. Muñoz-Leoz, B.; Ruiz-Romera, E.; Antigüedad, I.; Garbisu, C.; *Soil Biol. Biochem.* **2011**, *43*, 2176. [Crossref]
9. Song, W.; Ji, W.; Vantasin, S.; Tanabe, I.; Zhao, B.; Ozaki, Y.; *J. Mater. Chem. A* **2015**, *3*, 13556. [Crossref]
10. de Oliveira, R.; Martini, W. S.; Sant'Ana, A. C.; *Environ. Nanotechnol., Monit. Manage.* **2022**, *17*, 100657. [Crossref]
11. Marques, F. C.; Azevedo, G. C.; Senna, C. A.; Archanjo, B. S.; Corrêa, C. C.; Matos, R. C.; dos Santos, D. P.; Andrade, G. F. S.; *Spectrochim. Acta, Part A* **2022**, *272*, 120988. [Crossref]
12. Pilot, R.; Signorini, R.; Durante, C.; Orian, L.; Bhamidipati, M.; Fabris, L.; *Biosensors* **2019**, *9*, 57. [Crossref]
13. Teixeira, R. A. R.; Lima, F. R. A.; Silva, P. C.; Costa, L. A. S.; Sant'Ana, A. C.; *Spectrochim. Acta, Part A* **2019**, *223*, 117305. [Crossref]
14. Mungroo, N. A.; Oliveira, G.; Neethirajan, S.; *Microchim. Acta* **2016**, *183*, 697. [Crossref]
15. Chattopadhyay, S.; Sabharwal, P. K.; Jain, S.; Kaur, A.; Singh, H.; *Anal. Chim. Acta* **2019**, *1067*, 98. [Crossref]
16. Kołątaj, K.; Krajczewski, J.; Kudelski, A.; *Environ. Chem. Lett.* **2020**, *18*, 529. [Crossref]
17. Dowgiallo, A. M.; Guenther, D. A.; *J. Agric. Food Chem.* **2019**, *67*, 12642. [Crossref]
18. Jurašeková, Z.; Jutková, A.; Kožár, T.; Staničová, J.; *Spectrochim. Acta, Part A* **2022**, *268*, 120629. [Crossref]
19. Creighton, J. A.; Blatchford, C. G.; Albrecht, M. G.; *J. Chem. Soc. Faraday Trans. 2* **1979**, *75*, 790. [Crossref]
20. Darby, B. L.; Le Ru, E. C.; *J. Am. Chem. Soc.* **2014**, *136*, 10965. [Crossref]
21. Frisch, M. J.; Trucks, G. W.; Schlegel, H. B.; Scuseria, G. E.; Robb, M. B.; Cheeseman, J. R.; Scalmani, G.; Barone, V.; Petersson, G. A.; Nakatsuji, H.; Li, X.; Caricato, M.; Marenich, A.; Bloino, J.; Janesko, B. G.; Gomperts, R.; Mennucci, B.; Hratchian, H. P.; Ortiz, J. V.; Izmaylov, A. F.; Sonnenberg, J. L.; Williams-Young, D.; Ding, F.; Lipparini, F.; Egidi, F.; Goings, J.; Peng, B.; Petrone, A.; Henderson, T.; Ranasinghe, D.; Zakrzewski, V. G.; Gao, J.; Rega, N.; Zheng, G.; Liang, W.; Hada, M.; Ehara, M.; Toyota, K.; Fukuda, R.; Hasegawa, J.; Ishida, M.; Nakajima, T.; Honda, Y.; Kitao, O.; Nakai, H.; Vreven, T.; Throssel, K.; Montgomery Jr., J. A.; Peralta, J. E.; Ogliaro, F.; Bearpark, M.; Heyd, J. J.; Brothers, E.; Kudin, K. N.; Staroverov, V. N.; Keith, T.; Kobayashi, R.; Normand, J.; Raghavachari, K.; Rendell, Burant, J. C.; Iyengar, S. S.; Tomasi, J.; Cossi, M.; Millam, J. M.; Klene, M.; Adamo, C.; Cammi, R.; Ochterski, J. W.; Martin, R. L.; Morokuma, K.; Farkas, O.; Foresman, J. B.; Fox, D. J.; *Gaussian 09*, Wallingford, USA, 2016.
22. Ho, C.-H.; Lee, S.; *Colloids Surf., A* **2015**, *474*, 29. [Crossref]
23. Marques, F. C.; Alves, R. S.; dos Santos, D. P.; Andrade, G. F. S.; *Phys. Chem. Chem. Phys.* **2022**, *24*, 27449. [Crossref]
24. Jamróz, M. H.; *Vibrational Energy Distribution Anaysis: VEDA* 4; Warsaw, Poland, 2010. [Link] accessed in March 2023
25. European Food Safety Authority (EFSA); *EFSA J.* **2014**, *12*, 3485. [Crossref]
26. Teixeira, R. A. R.; Costa, L. A. S.; Sant'Ana, A. C.; *J. Raman Spectrosc.* **2019**, *50*, 1462. [Crossref]
27. Alves, A. P. P.; de Sena, L. Á.; Archanjo, B. S.; de Oliveira, L. F. C.; Dantas, S. O.; Sant'Ana, A. C.; *Vib. Spectrosc.* **2013**, *64*, 153. [Crossref]
28. Moskovits, M.; DiLella, D. P.; Maynard, K. J.; *Langmuir* **1988**, *4*, 67. [Crossref]
29. Moskovits, M.; Suh, J. S.; *J. Phys. Chem.* **1984**, *88*, 5526. [Crossref]
30. Gamberini, M. C.; Mary, Y. S.; Mary, Y. S.; Krátký, M.; Vinsova, J.; Baraldi, C.; *Spectrochim. Acta, Part A* **2021**, *248*, 119265. [Crossref]
31. Firkala, T.; Tálas, E.; Kristyán, S.; Szöll'si, G.; Drotár, E.; Mink, J.; Mihály, J.; *J. Raman Spectrosc.* **2015**, *46*, 1102. [Crossref]
32. Filgueiras, A. L.; Lima, F. R. A.; de Carvalho, D. F.; Meirelles, M. A.; Paschoal, D.; dos Santos, H. F.; Sanchez-Cortes, S.; Sant'Ana, A. C.; *Vib. Spectrosc.* **2016**, *86*, 75. [Crossref]

33. Webster, G. R.; Bisset, N. B.; Cahill, D. M.; Jones, P.; Killick, A.; Hawley, A.; Boyd, B. J.; *J. Agric. Food Chem.* **2016**, *64*, 6139. [Crossref]
34. Sánchez-Cortés, S.; García-Ramos, J. V.; *Surf. Sci.* **2001**, *473*, 133. [Crossref]
35. Rubim, J. C.; Trindade, F. A.; Gelesky, M. A.; Aroca, R. F.; Dupont, J.; *J. Phys. Chem. C* **2008**, *112*, 19670. [Crossref]

Submitted: November 18, 2022
Published online: March 23, 2023